

## Article

# A Study of the Metabolic Profiles of *Penicillium dimorphosporum* KMM 4689 Which Led to Its Re-Identification as *Penicillium hispanicum*

Liliana E. Nesterenko<sup>1,2</sup>, Roman S. Popov<sup>1</sup>, Olesya I. Zhuravleva<sup>1,2</sup>, Natalya N. Kirichuk<sup>1</sup>, Viktoria E. Chausova<sup>1</sup>, Kirill S. Krasnov<sup>3</sup>, Mikhail V. Pivkin<sup>1</sup>, Ekaterina A. Yurchenko<sup>1</sup>, Marina P. Isaeva<sup>1</sup> and Anton N. Yurchenko<sup>1,\*</sup>

<sup>1</sup> G.B. Elyakov Pacific Institute of Bioorganic Chemistry Far Eastern Branch of Russian Academy of Science, Prospect 100-Letiya Vladivostoka, 159, 690022 Vladivostok, Russia

<sup>2</sup> Institute of High Technologies and Advanced Materials, Far Eastern Federal University, 10 Ajax Bay, Russky Island, 690922 Vladivostok, Russia

<sup>3</sup> Institute of Theoretical and Experimental Biophysics, Russian Academy of Sciences, Institutskaya ul., 3, 142290 Pushchino, Russia

\* Correspondence: yurchenkoan@piboc.dvo.ru

**Abstract:** Changes in cultivation conditions, in particular salinity and temperature, affect the production of secondary fungal metabolites. In this work, the extracts of fungus previously described as *Penicillium dimorphosporum* cultivated in various salinity and temperature conditions were investigated using HPLC UV/MS techniques, and their DPPH radical scavenging and cytotoxicity activities against human prostate cancer PC-3 cells and rat cardiomyocytes H9c2 were tested. In total, 25 compounds, including 13 desoxyisoaustamide-related alkaloids and eight anthraquinones, were identified in the studied extracts and their relative amounts were estimated. The production of known neuroprotective alkaloids **5**, **6** and other brevianamide alkaloids was increased in hypersaline and high-temperature conditions, and this may be an adaptation to extreme conditions. On the other hand, hyposalinity stress may induce the synthesis of unidentified antioxidants with low cytotoxicity that could be very interesting for future investigation. The study of secondary metabolites of the strain KMM 4689 showed that although brevianamide-related alkaloids and anthraquinone pigments are widely distributed in various fungi, these metabolites have not been described for *P. dimorphosporum* and related species. For this reason, the strain KMM 4689 was re-sequenced using the  $\beta$ -tubulin gene and ITS regions as molecular markers and further identified as *P. hispanicum*.

**Keywords:** *Penicillium dimorphosporum*; *Penicillium hispanicum*; OSMAC; HPLC MS; metabolite profile; ITS;  $\beta$ -tubulin; phylogeny; re-identification; bioactivity; cultivation conditions; salinity; secondary metabolites; PCA



**Citation:** Nesterenko, L.E.; Popov, R.S.; Zhuravleva, O.I.; Kirichuk, N.N.; Chausova, V.E.; Krasnov, K.S.; Pivkin, M.V.; Yurchenko, E.A.; Isaeva, M.P.; Yurchenko, A.N. A Study of the Metabolic Profiles of *Penicillium dimorphosporum* KMM 4689 Which Led to Its Re-Identification as

*Penicillium hispanicum*. *Fermentation* **2023**, *9*, 337. <https://doi.org/10.3390/fermentation9040337>

Academic Editor: Francesca Berini

Received: 28 January 2023

Revised: 23 March 2023

Accepted: 24 March 2023

Published: 28 March 2023



**Copyright:** © 2023 by the authors. Licensee MDPI, Basel, Switzerland. This article is an open access article distributed under the terms and conditions of the Creative Commons Attribution (CC BY) license (<https://creativecommons.org/licenses/by/4.0/>).

## 1. Introduction

Marine microorganisms have received increasing attention due to their features of metabolism, which have been acquired as an adaptation to prevailing extreme conditions in the marine environment [1]. The versatility of metabolic pathways helps filamentous fungi to adapt to changing environmental conditions and can be used to achieve the tasks of the biotechnological production of drugs [2]. Changing the cultivation conditions such as the composition of nutrients, salinity, pH and temperature is one of the options for the OSMAC (one strain–many compounds) approach for the investigation of fungal secondary metabolites [3]. It was first formulated 20 years ago [4] and has proved to be very effective since [5]. For example, cultivation of *Aspergillus aculeatus* strain in high-salinity conditions resulted in the up-regulation of aspergillusol, secalonic acid D and aculens C and D production [6]. A high level of NaCl in a culture of *Asteromyces cruciatus* induced the

production of new metabolite primarolide A, and additional using of epigenetic modifier suberoylanilide hydroxamic acid resulted in new primarolide B isolation [7].

Previously, we found that the marine coral-derived strain of fungus *Penicillium dimorphosporum* produces a number of new deoxyisoaustamide alkaloids with neuroprotective or cytotoxic properties [8,9]. Interestingly, the neuroprotective effect against paraquat toxicity is observed only for 16,17-dihydroxy-deoxydihydroisoaustamide derivatives. Of course, many secondary metabolites from micro- and macroorganisms and their synthetic derivatives have shown neuroprotective or cytotoxic activity. Therefore, the need for a more detailed study of yet another neuroprotective or anticancer natural compound can be questioned. However, it is clear that with a greater number of molecules with a well-established mechanism of action available, more effective development of real drugs through modern methods of bioinformatics and drug design can be realized. Additionally, from this point of view, these compounds are of particular interest. However, the low production of these substances by the fungus makes the study of their bioactivity very limited.

Thus, this study aimed to investigate how the change in culture conditions of the marine fungus *Penicillium dimorphosporum* KMM 4689 affects the production of known bioactive compounds and other secondary metabolites of this fungus.

## 2. Materials and Methods

### 2.1. General Experimental Procedures

Microscopic examination and photography of fungal cultures were performed with an Olympus CX41 microscope fitted with an Olympus SC30 digital camera. Detailed examination of ornamentation of the fungal conidia was performed using scanning electron microscopy (SEM) EVO 40.

Low-pressure liquid column chromatography was performed using a Gel ODS-A (12 nm, S—75  $\mu$ m, YMC Co., Ishikawa, Japan). Plates precoated with Si gel (5–17  $\mu$ m, 4.5 cm  $\times$  6.0 cm, Imid Ltd., Krasnodar, Russia) were used for thin-layer chromatography.

### 2.2. Fungal Strain

The fungal strain was isolated from unidentified soft coral sample collected in the South China Sea (Con Co Island, Vietnam) during the 49th expedition of the R/V *Akademik Oparin*. The strain was earlier identified based on molecular features (ITS regions) as *Penicillium dimorphosporum* [8]. The fungal strain is stored in the Collection of Marine Microorganisms (PIBOC FEB RAS, Vladivostok, Russia) under the code KMM 4689 and in the Collection of Nhatrang Institute of Technology Research and Applications under the code VO49-30.5.

### 2.3. Cultivation of Fungus

The fungus was cultured for 21 days at 22 °C or 30 °C in 500 mL Erlenmeyer flasks, each containing rice (20.0 g), yeast extract (20.0 mg),  $\text{KH}_2\text{PO}_4$  (10 mg) and various amount of sea salt. Detailed fermentation conditions are described in Table 1. Sea salt was obtained through evaporation of natural sea water (Vodolaznaya bay, Troitsa bay, the Sea of Japan, April 2021). The natural salinity of the water used was 37.8 mg/mL.

**Table 1.** Cultivation conditions of *Penicillium dimorphosporum* KMM 4689.

No	Cultivation Conditions	Sample Code	EtOAc Extract Amount, mg	Purified Extract Amount, mg
1	22 °C, sea water	22-sw	452.3	178.1
2	22 °C, sea salt (5 mg/mL)	22-5	536.9	211.4
3	22 °C, sea salt (10 mg/mL)	22-10	246.2	96.6
4	22 °C, sea salt (15 mg/mL)	22-15	259.5	34.8
5	22 °C, sea salt (20 mg/mL)	22-20	374.3	47.0
6	22 °C, sea salt (25 mg/mL)	22-25	344.3	32.3
7	22 °C, sea salt (30 mg/mL)	22-30	343.6	23.3
8	22 °C, sea salt (40 mg/mL)	22-40	294.5	31.7
9	22 °C, sea salt (45 mg/mL)	22-45	151.8	22.2
10	22 °C, sea salt (50 mg/mL)	22-50	391.1	50.6
11	30 °C, sea water	30-sw	409.4	161.2
12	30 °C, sea salt (5 mg/mL)	30-5	415.8	163.7
13	30 °C, sea salt (10 mg/mL)	30-10	294.3	114.4
14	30 °C, sea salt (15 mg/mL)	30-15	408.4	53.6
15	30 °C, sea salt (20 mg/mL)	30-20	337.5	44.3
16	30 °C, sea salt (25 mg/mL)	30-25	311.5	47.8
17	30 °C, sea salt (30 mg/mL)	30-30	358.0	32.8
18	30 °C, sea salt (40 mg/mL)	30-40	268.1	30.5
19	30 °C, sea salt (45 mg/mL)	30-45	155.2	22.7
20	30 °C, sea salt (50 mg/mL)	30-50	142.1	29.4

#### 2.4. Extraction

At the end of the incubation period, each mycelium and medium were homogenized and extracted with EtOAc ( $2 \times 75$  mL). The obtained extracts were concentrated to dryness. The residues (Table 1) were dissolved in methanol and purified using column chromatography on a Gel ODS-A in methanol.

#### 2.5. HPLC UV

HPLC UV was carried out on an Agilent 1260 Infinity II chromatograph with a UV detector Agilent 1260 VWD (Agilent Technologies, Waldbronn, Germany) using a Supelco Discovery C-18 analytical column (5  $\mu$ m, 4.6 mm  $\times$  250 mm) in a methanol/water gradient (20% MeOH—10 min, 20–100% MeOH—30 min, 100–20% MeOH—5 min). Detection was performed at 220 and 290 nm. The extract concentration was 2 mg per 30  $\mu$ L for injection. The flow rate was 0.8 mL/min. A qualitative and quantitative analysis of HPLC UV chromatograms was performed using Agilent OpenLab software (version 2.4). The obtained data were exported into MS Excel for further calculation of the number of peaks and their total area. Peaks with a relative area less than 1% were considered noise and were eliminated.

#### 2.6. HPLC MS

Analysis was performed using a Bruker Elute UHPLC chromatograph (Bruker Daltonics, Bremen, Germany) connected to a Bruker Impact II Q-TOF mass spectrometer (Bruker Daltonics, Bremen, Germany). An InfinityLab Poroshell 120 SB-C18 column (2.1 mm  $\times$  150 mm, 2.7  $\mu$ m, Agilent Technologies, Santa Clara, CA, USA) was used for chromatographic separation. The mobile phases were 0.1% formic acid in H<sub>2</sub>O (eluent A) and 0.1% formic acid in MeCN (eluent B). The gradient program was as follows: from 10% to 45% eluent B from 0 to 10 min, from 45% to 100% eluent B from 10 to 20 min, isocratic at 100% of eluent B from 20 to 25 min, from 100% to 10% eluent B from 25 to 25.2 min. After returning to the initial conditions, the equilibrium was achieved after 5 min. Chromatographic separation was performed at a 0.4 mL/min flow rate at 40 °C. The injection volume was 2  $\mu$ L.

The mass spectrometry detection was performed using an ESI ionization source in positive ion mode. The optimized ionization parameters for ESI were as follows: a capillary voltage of 4.5 kV, nebulization with nitrogen at 2.5 bar, dry gas flow of 6 L/min at a temperature of 200 °C. The mass spectra were recorded within an  $m/z$  mass range of 50–2000 (scan time 1 s). Collision-induced dissociation (CID) product ion mass spectra were recorded in auto-MS/MS mode with a collision energy ranging from 15 eV at 100  $m/z$  to 120 eV at 1500  $m/z$  (the exact collision energy setting depended on the molecular masses of precursor ions). The precursor ions were isolated with an isolation width of 4 Th.

The mass spectrometer was calibrated using the ESI-L Low Concentration Tuning Mix (Agilent Technologies, Santa Clara, CA, USA). The instrument was operated using otofControl (ver. 4.1, Bruker Daltonics, Bremen, Germany) and data were analyzed using the DataAnalysis Software (ver. 4.4, Bruker Daltonics, Bremen, Germany).

### 2.7. Data Analysis

UHPLC-Q-TOF data were converted from Bruker “.d” formatting to “.mzXML” using MSConvert 3.0 (part of ProteoWizard 3.0 package, Palo Alto, California, USA) [10] and further processing was performed with MZMine (version 2.53) [11]. The MZMine processing settings were as follows: mass detection was carried out at the MS1 level and MS2 level with noise level thresholds of 60 and 40, respectively. Chromatograms were made with the ADAP Chromatogram Builder Module [12] with the following parameters: min group size in # of scans was set to 6, group intensity threshold and min highest intensity were set to 130 and 300, respectively,  $m/z$  tolerance was set to 0.05  $m/z$ . The chromatogram deconvolution module was used with the ADAP algorithm with a signal/noise threshold of 8, min feature height of 300, coefficient/area threshold of 40, peak duration range was set from 0 to 2.0 and RT wavelet range was set from 0 to 0.1. The  $m/z$  center calculation was set to MEDIAN. The Isotopics peaks grouper module was used with an  $m/z$  tolerance of 5 ppm, retention time tolerance of 0.1 min, the monotonic shape function set to true, a maximum charge of 2 and the representative isotope set to the most intense. Alignment was achieved with the Join aligner function with an  $m/z$  tolerance of 5 ppm, a weight for  $m/z$  at 50, a retention time tolerance of 0.1 min and a weight for RT at 50. The Require same charge state, Require same ID and the Compare spectra similarity functions were set to false. The aligned feature list was exported by the Export/Submit to “GNPS-FBMN” module with the Merge MS/MS (experimental) function with the following parameters: Select spectra to merge was set to across samples, the  $m/z$  merge mode was set to weighted average (remove outliers), the intensity merge mode was set to sum intensities, the expected mass deviation was set to 5 ppm, the cosine threshold was set to 70%, the peak count threshold was set to 20%, the isolation window offset ( $m/z$ ) was set to 0 and the isolation window width ( $m/z$ ) was set to 3.

### 2.8. Molecular Networking and Spectral Library Search

Feature-based molecular networking (FBMN) was generated with the pre-processed data on the Global Natural Products Social Molecular Networking (GNPS) website (<https://gnps.ucsd.edu>, accessed on 24 October 2022) [13,14]. The molecular networking module was used to visualize the molecular network. The precursor ion mass tolerance and fragment ion mass tolerance were both set to 0.02 Da. The network edges were set to have a cosine score of 0.4 or above, with a minimum of three matched peaks. The next parameters were also specified: minimum matched fragment ions and minimum cluster size were both set to 4. Other parameters were maintained as default. Annotation of the MS/MS spectra was carried out with the DEREPLICATOR tool. Visualization of the network was carried out with Cytoscape 3.9.1 [15].

Dereplication of the MS/MS spectra was carried out using the GNPS module Library Search. All parameters were maintained as default.

Metabolite dereplication was also carried out with an in-house MS/MS spectral library, comparing experimental spectra and retention times (RT) with the spectra and RT obtained for reference compounds 1–10 [8].

### 2.9. Principal Component Analysis (PCA)

PCA was performed using the python package Scikit-Learn (v.1.2.1) [16]. A PCA model was established to assess the distribution of samples and based on detected metabolites in each sample. Visualization of principal component plot was performed using the python package bioinfokit (v.2.1.0) [17].

### 2.10. Bioassays

#### 2.10.1. Cell Culture

The human prostate cancer cells PC-3 were purchased from ATCC (American Type Culture Collection, Manassas, VA, USA). The rat cardiomyocytes H9c2 cells were kindly provided by Prof. Dr. Gunhild von Amsberg from Martini-Klinik Prostate Cancer Center, University Hospital Hamburg-Eppendorf, Hamburg, Germany. The PC-3 and H9c2 cells were cultured in DMEM containing 10% fetal bovine serum (Biolog, St. Petersburg, Russia) and 1% penicillin/streptomycin (Biolog, St. Petersburg, Russia) at 37 °C in a humidified atmosphere with 5% (*v/v*) CO<sub>2</sub>. The cells were incubated in cultural flasks until sub-confluent (~80%).

#### 2.10.2. Cell Viability Assay

The PC-3 cells ( $5 \times 10^3$  cells/well) and H9c2 cells ( $3 \times 10^3$  cells/well) were seeded in a 96-well plate and incubated overnight. Then, the extracts at a concentration of 10 µg/mL were added and the cells were further incubated for an additional 24 h. After that, cell viability was determined using the MTT (3-(4,5-dimethylthiazol-2-yl)-2,5-diphenyltetrazolium bromide) method according to the manufacturer's instructions (Sigma-Aldrich, St. Louis, MO, USA). Absorbance of the converted formazan was measured using a Multiskan FC microplate photometer (Thermo Scientific, Waltham, MA, USA) at  $\lambda = 570$  nm. The results are presented as percentages of control data.

#### 2.10.3. Cell-Free DPPH Assay

The extract solutions at a concentration of 1.25 µg/mL (120 µL) were dispensed into the wells of a 96-well microplate. In total, 30 µL of the DPPH (Sigma-Aldrich, Steinheim, Germany) solution in MeOH ( $1.5 \times 10^{-4}$  M) was added to each well. Concentrations of compounds in the mixture were 1 µg/mL. Pure DMSO was used as a control. The mixture was shaken and left to stand for 30 min, and the absorbance of the resulting solution was measured at 520 nm with a microplate reader MultiskanFC (Thermo Scientific, USA). The radical scavenging activity of all extracts is presented as per cent of DMSO data.

### 2.11. DNA Extraction and Amplification

Genomic DNA was isolated from fungal mycelium grown on MEA (malt extract agar) at 25 °C for 7 days, using the MagJET Plant Genomic DNA Kit (Thermo Fisher Scientific, Waltham, MA, USA), according to the manufacturer's protocol. PCR was conducted using GoTaq Flexi DNA Polymerase (Promega, Madison, WI, USA). For amplification of the internal transcribed spacer (ITS) region, the primer pair 1400-F (5'-CTGCCCTTTGTACACACCGCCCGTC-3') [18] and D2CR (5'-CCCTGGTCCGTGTTTCAAGA-3') was used [19]. The reaction profile was 95 °C for 300 s, 35 cycles of 94 °C for 20 s, 55 °C for 20 s, and 72 °C for 90 s and finally 72 °C for 300 s. For amplification of the partial beta/ $\beta$ -tubulin gene region, the primer pair Bt-2a and Bt-2b was used [20]. The reaction profile was 95 °C for 300 s, 35 cycles of 94 °C for 20 s, 55 °C for 20 s, and 72 °C for 60 s and finally 72 °C for 300 s. The amplified ITS region and partial beta/ $\beta$ -tubulin genes were purified with the ExoSAP-IT™ PCR Product Cleanup Reagent (Thermo Fisher Scientific, Waltham, MA, USA). Sequencing was bidirectional performed with the same primers on an Applied Biosystems SeqStudio Genetic Analyzer

(Thermo Fisher Scientific, Waltham, MA, USA) using the Big Dye Terminator reagent kit, version 3.1. Gene sequences were deposited in GenBank under accession numbers MW325972 for the ITS gene region and OP407668 for the partial  $\beta$ -tubulin gene region (Table 2).

**Table 2.** Strains used in phylogenetic analysis and GenBank accession numbers of ITS and  $\beta$ -tubulin molecular data.

Taxon	Collection Number	GenBank Accession Number	
		ITS	$\beta$ -Tubulin
<i>Penicillium canis</i> S.W. Peterson	NRRL 62,798 <sup>T</sup>	KJ511291	
<i>Penicillium capsulatum</i> Raper et Fennell	CBS 301.48 <sup>T</sup>	AF033429	MN969375
<i>Penicillium catenatum</i> D.B. Scott	CBS 352.67 <sup>T</sup>	KC411754	
<i>Penicillium cyaneum</i> (Bainier et Sartory) Biourge	CBS 315.48 <sup>T</sup>	AF033427	JX091552
<i>Penicillium dimorphosporum</i> H.J. Swart	CBS 456.70 <sup>T</sup>	AF081804	
<i>Penicillium erubescens</i> D.B. Scott	CBS 318.67 <sup>T</sup>	AF033464	
<i>Penicillium georgiense</i> S.W. Peterson et B.W. Horn	CBS 132826 <sup>T</sup>	EF422852	EF506223
<i>Penicillium guttulatum</i> J.C. Gilman et E.V. Abbott	NRRL 907 <sup>T</sup>	HQ646592	
<i>Penicillium hermansii</i> Houbraken, Seifert et Samson	CBS 124,296 <sup>T</sup>	MG333472	
<i>Penicillium hispanicum</i> C. Ramírez, A.T. Martínez et Ferrer	KMM 4689	MW325972	OP407668
	CBS 691.77 <sup>T</sup>	JX841247	KJ834456
<i>Penicillium laeve</i> (K. Ando et Manoch) Houbraken et Samson	CBS 136,665 <sup>T</sup>	KF667369	
<i>Penicillium menonorum</i> S.W. Peterson	NRRL 50,410 <sup>T</sup>	HQ646591	
<i>Penicillium nepalense</i> Takada et Udagawa	CBS 203.84 <sup>T</sup>	KC411692	
<i>Penicillium ornatum</i> Udagawa	CBS 190.68 <sup>T</sup>	KC411687	KJ834479
<i>Penicillium ovatum</i> (K. Ando et Nawawi) Houbraken et Samson	CBS 136,664 <sup>T</sup>	KF667370	
<i>Penicillium parvofructum</i> Guevara-Suarez, Cano-Canals, Cano et Stchigel	CBS 141,690 <sup>T</sup>	AF033460	
	CBS 359.48 <sup>T</sup>	AF033460	
<i>Penicillium pumilum</i> Raper et Fennell	CBS 102,479 <sup>T</sup>	AF037431	
<i>Penicillium ramusculum</i> Bat. et H. Maia	CBS 251.56 <sup>T</sup>	EF433765	EU427269
<i>Penicillium rubidurum</i> Udagawa et Y. Horie	CBS 609.73 <sup>T</sup>	AF033462	
<i>Penicillium striatisporum</i> Stolk	CBS 705.68 <sup>T</sup>	AF038938	
<i>Penicillium vinaceum</i> J.C. Gilman et E.V. Abbott	CBS 389.48 <sup>T</sup>	AF033461	
<i>Talaromyces marneffeii</i> (Segretain, Capponi et Sureau) Samson, N. Yilmaz, Frisvad et Seifert	CBS 388.87 <sup>T</sup>	JN899344	JX091389

<sup>T</sup>—ex-type strain.

### 2.12. Phylogenetic Analysis

The ITS region and partial  $\beta$ -tubulin gene sequences were aligned with MEGA X software version 11.0.9 [21] using the Clustal W algorithm. The available homologs were searched in the GenBank database (<http://ncbi.nlm.nih.gov>, accessed on 15 September 2022) using the BLASTN algorithm (<http://www.ncbi.nlm.nih.gov/BLAST>, accessed on 15 September 2022). The phylogenetic analysis was conducted using MEGA X software [21]. The ITS region and partial  $\beta$ -tubulin gene sequences were concatenated into one alignment. A phylogenetic tree was constructed according to the maximum likelihood (ML) algorithm based on the Tamura–Nei model [22]. The topology of the tree was evaluated with 1000 bootstrap replicates. *Talaromyces marneffeii* was used in the phylogenetic analysis as the outgroup (Table 2).

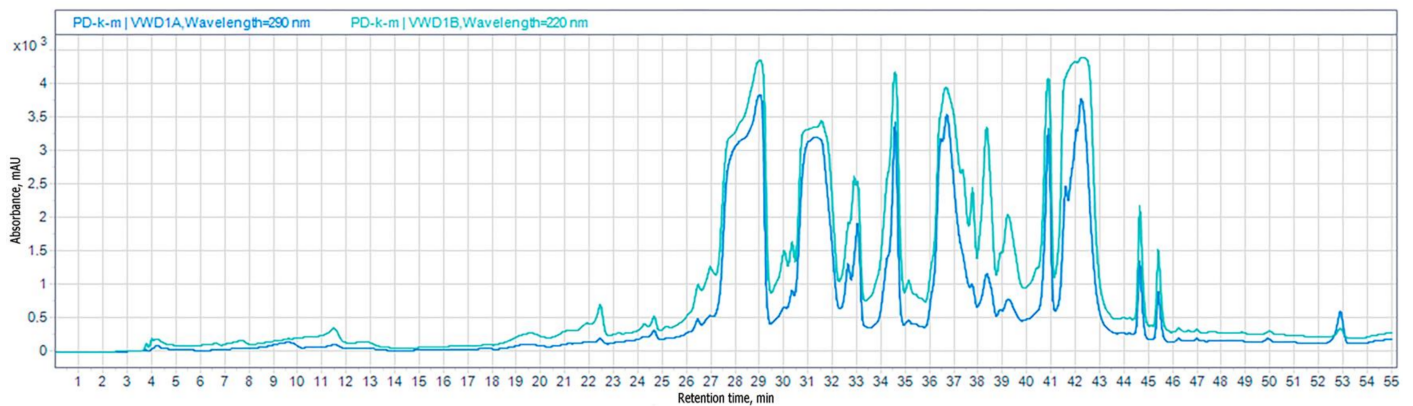
The ITS region sequences of members of the genus *Penicillium* section *Ramigena* series *Ramigena* and section *Exilicaulis* series *Erubescens* were aligned using the Clustal W algorithm. The ML tree of ITS region sequences was reconstructed based on the Tamura–Nei model [22] and evaluated with 1000 bootstrap replicates.

### 3. Results

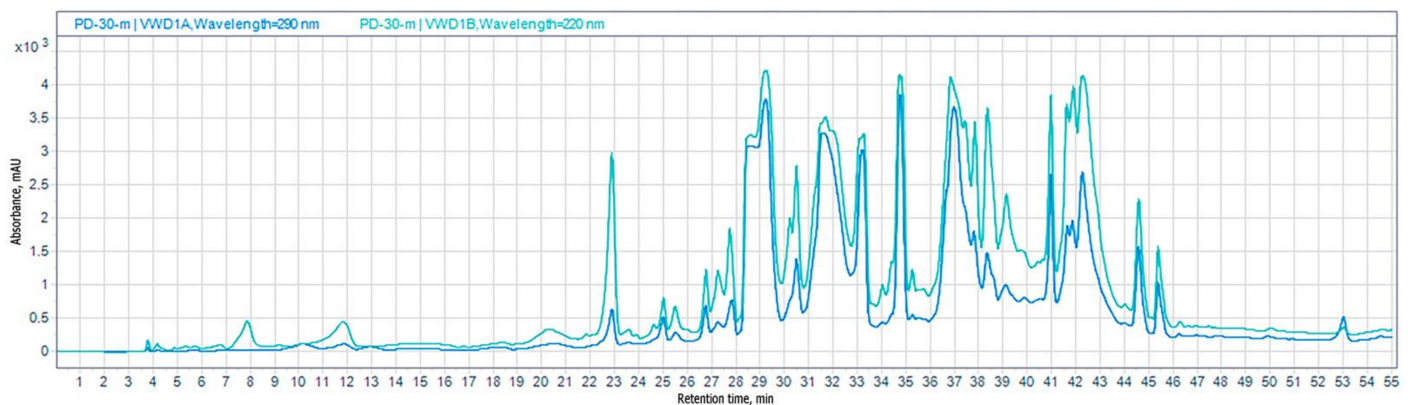
#### 3.1. The Effect of Culture Conditions on Metabolic Profile of Fungal Extracts and Its Bioactivity

##### 3.1.1. HPLC UV

The purified extracts were analyzed through HPLC UV at 290 and 220 nm. The chromatograms of extracts from fungus cultivated with sea water at 22 °C and at 30 °C are presented in Figure 1 and other chromatograms are shown in the Supplementary Materials (Figures S1–S20).



(A)



(B)

**Figure 1.** HPLC UV chromatograms of extracts from fungus cultivated with sea water at 22 °C (A), and at 30 °C (B). Chromatograms were recorded at 290 nm (blue) and 220 nm (green).

The HPLC UV data showed that cultivation at 30 °C resulted in a more varied metabolite profile of fungal extract, especially in the polar field.

Each chromatogram was divided into three zones: polar (0–30 min, 20%–70% of MeOH), mid-polar (30–40 min, 70%–100% of MeOH) and non-polar (40–55 min, 100% MeOH). The total number of peaks in each zone and their total area were calculated and are presented in Figures 2 and 3, respectively.

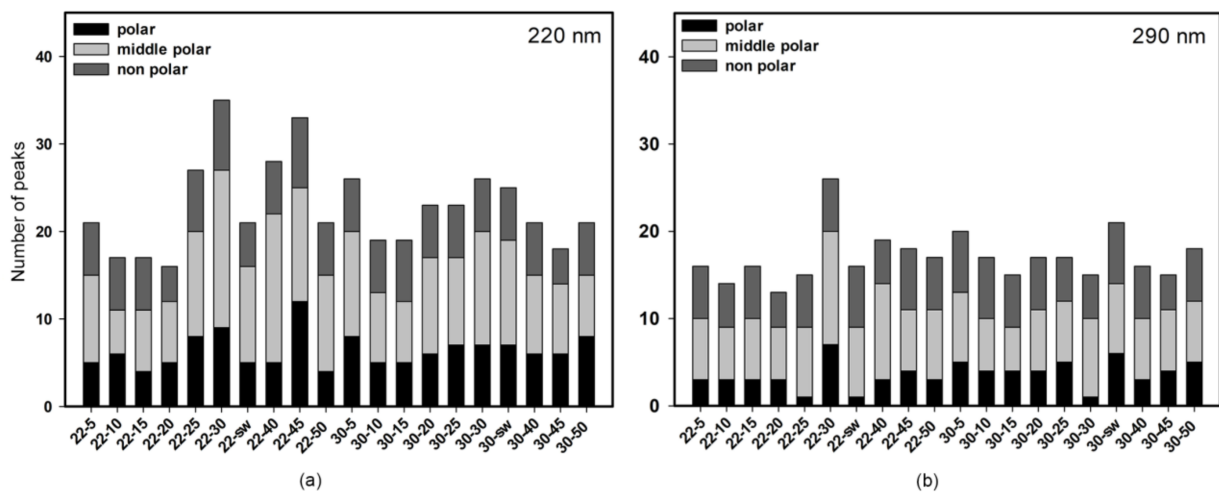


**Figure 2.** Total number of peaks in HPLC UV chromatograms. (a) Detection at 220 nm; (b) detection at 290 nm. The codes of extracts are presented in X axes of graphs.

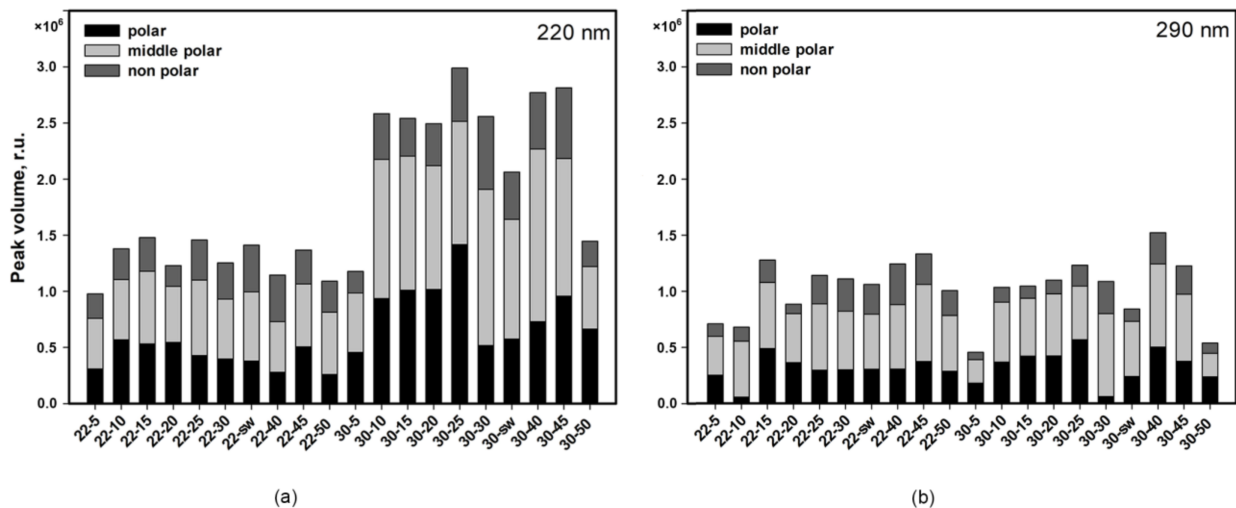


**Figure 3.** Total area of peaks in HPLC UV chromatograms. (a) Detection at 220 nm; (b) detection at 290 nm. The codes of extracts are presented in X axes of graphs.

A change in the concentration of sea salt during cultivation at both 22 °C and 30 °C had no significant effect on the number of peaks in the non-polar region.

Reducing the concentration of sea salt from 30 to 10 mg/mL (hypo salinity) at 22 °C led to a decrease in the number of peaks in the mid-polar region. The number of peaks in this region for fungal extracts cultivated at 30 °C and with a decrease in sea salt concentration from 30 to 10 mg/mL also decreased. However, with a further decrease in the salt concentration from 10 to 5 mg/mL, the number of peaks increased.

An increase in the concentration of sea salt at 22 °C hardly changed the number of peaks in the mid-polar region, while an increase in the concentration of sea salt at 30 °C caused a decrease in the number of such peaks.

The greatest changes in the number of peaks were observed in the polar region of the chromatograms.

A slight decrease in sea salt concentration to 20–25 mg/mL at 22 °C led to an increase in the number of peaks, and with a further decrease in the salt concentration, the number of peaks was similar to the base conditions (natural sea water). At an increased cultivation temperature, a decrease in the concentration of sea salt led to a gradual increase in the number of peaks, reaching the highest value at 5 mg/mL. This was observed at both wavelengths.

Increasing the sea salt concentration to 45 mg/mL at 22 °C resulted in a significant increase in the number of peaks, but a further increase to 50 mg/mL resulted in a decrease in the number of peaks. Increasing the concentration of sea salt at 30 °C did not lead to any noticeable change at a wavelength of 220 nm, but caused a decrease in the number of peaks at 290 nm.

The change in the total area of the peaks with a change in the conditions for the fungus cultivation was especially noticeable in the polar zone. A decrease in the salt concentration at 22 °C led to slight fluctuations in the areas of these peaks, recorded at 220 nm. At the same time, a decrease in the salt concentration to 5–10 mg/mL at 22 °C led to a significant decrease in the areas of the peaks at 290 nm.

A change in the salt concentration at 30 °C also led to nonlinear changes in the area of the peaks in the polar region at both wavelengths. Changes in peak area in the mid-polar and non-polar regions were small except for extracts of the fungus cultivated at 5 and 50 mg/mL. In these cases, a sharp decrease in the area of the peaks was observed over the entire range of polarity, and this was recorded at both wavelengths. At the same time, the masses of these extracts were similar to the masses of extracts obtained using natural sea water, and significantly higher than at all other sea salt concentrations.

Thus, HPLC UV data showed that the cultivation conditions significantly change the metabolite profiles of fungal extracts.

### 3.1.2. Bioactivity of Extracts

The scavenging activity of all extracts for DPPH radicals in cell-free tests as well as their cytotoxic effects on human prostate cancer PC-3 and rat normal cardiomyocytes H9c2 line are presented in Table 3.

**Table 3.** The cytotoxic and radical scavenging activities of fungal extracts.

Extract Code	Cell Viability <sup>1</sup> , % of Control		DPPH Radicals <sup>2</sup> , %
	PC-3	H9c2	
22-5	85.4 ± 0.8	93.5 ± 3.8	19.9 ± 0.9
22-10	56.6 ± 7.6	70.1 ± 10.2	20.4 ± 2.3
22-15	56.8 ± 9.6	46.6 ± 0.7	25.8 ± 1.8
22-20	64.8 ± 6.5	67.2 ± 5.6	26.9 ± 4.1
22-25	46.0 ± 8.1	67.1 ± 8.6	29.5 ± 3.1
22-30	56.4 ± 4.7	57.9 ± 4.1	40.7 ± 8.0
22-sw	44.2 ± 6.6	53.2 ± 2.2	39.6 ± 2.5
22-40	60.3 ± 4.4	57.9 ± 6.2	28.4 ± 2.4
22-45	68.3 ± 5.0	64.8 ± 4.7	35.3 ± 5.0
22-50	27.7 ± 4.0	64.4 ± 4.1	19.1 ± 1.8
30-5	67.6 ± 9.5	70.5 ± 3.1	16.2 ± 4.0
30-10	62.6 ± 6.4	65.4 ± 2.1	23.1 ± 2.4
30-15	70.2 ± 2.6	67.0 ± 2.5	40.1 ± 4.6
30-20	77.4 ± 12.2	70.9 ± 4.4	29.1 ± 2.2
30-25	74.4 ± 5.4	75.1 ± 0.8	31.9 ± 1.9
30-30	48.1 ± 6.6	73.5 ± 5.2	33.1 ± 5.2
30-sw	70.9 ± 1.2	62.7 ± 3.6	21.4 ± 5.2
30-40	50.5 ± 10.7	82.3 ± 6.4	31.0 ± 8.3
30-45	53.4 ± 1.0	69.8 ± 1.0	36.9 ± 9.3
30-50	86.9 ± 2.8	72.2 ± 2.2	42.9 ± 3.2

<sup>1</sup> The concentrations of extracts were 10 µg/mL. <sup>2</sup> The concentrations of extracts were 1 µg/mL. All data are presented as a mean ± standard error of mean (SEM).

The DPPH radical scavenging activity of all tested extracts was different. From the extracts of fungus cultivated at 22 °C, a weak activity was observed for the 22-30 and 22-sw extracts. The extracts from 22-10 to 22-45 showed middle activity and the 22-5 and 22-50 extracts showed the most DPPH radical scavenging effect. From the extracts of fungus cultivated at 30 °C, most active extracts were also 30-5. The extracts from 30-15 to 30-45

showed moderate DPPH radical scavenging effects and extracts 30-15 and 30-50 shown weak activity in this test.

The cytotoxic activity of the extracts was not high. Most of the extracts decreased PC-3 and H9c2 cells viability by 23–50%. Extract 22-50 decreased the viability of PC-3 cells by 72%, while it decreased H9c2 cell viability by only 37%. Surprisingly, extract 22-5 showed minimal cytotoxicity against both cell lines.

The hyposalinity as well as hypersalinity at 22 °C resulted in higher DPPH radical scavenging activity of the extracts. The hyposalinity conditions, but not hypersalinity, at 30 °C also increased the DPP-radical scavenging activity of extracts. Similar conclusions about the influence of culture conditions on the cytotoxic activity of the extracts cannot be drawn.

### 3.1.3. HPLC MS

For detailed analysis of the metabolite profiles, the extracts of fungal cultures at 22 °C and 30 °C with 5, 15, 37.8 (sw) and 50 µg/mL of sea salt were studied using the HPLC MS method. The UHPLC MS chromatogram of the 22-sw extract as an example is presented in Figure 4 and chromatograms of the 22-5, 22-15, 22-50, 30-5, 30-15, 30-sw and 30-50 extracts are presented in Figures S21–S28.

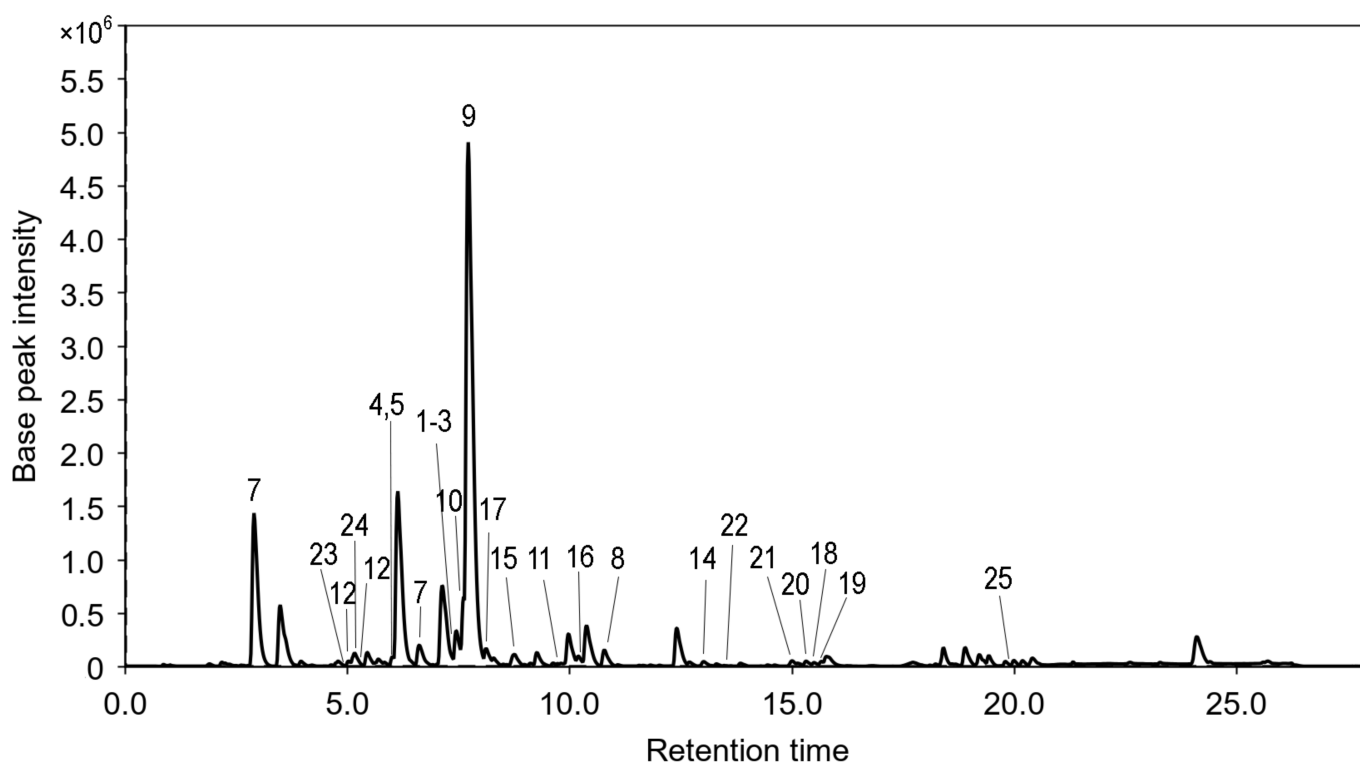


**Figure 4.** UHPLC MS chromatogram of extract 22-sw.

In total, 25 known compounds such as indole-diketopiperazine alkaloids 1–13, anthraquinone derivatives emodine (14) [23], citreosein (15) [24], 2-chlorocitreosein (16) [25], endocrocin (17) [26] and nephrolaevigatins A–D (18–21) [27], secalonic acid D (22) [28], cinnamic acid (23) and isochromen (24) derivatives and unidentified ergostane derivative (25) (Figure 4, Appendix A) were identified in various combination in the studied extracts.

The main peak in all obtained HPLC MS chromatograms was detected at 7.7 min. The base peak with  $m/z$  348.1697 corresponded to the molecular formula  $C_{21}H_{21}N_3O_2$ , the same as (+)-deoxyisoaustamide (9), which was previously isolated from this strain. This

was additionally proven through comparison of experimental MS/MS spectra and RT with an in-house database (Figure S37).

The peak detected at 2.9 min with  $m/z$  364.1645 corresponded to the molecular formula  $C_{21}H_{21}N_3O_3$ , the same as 3 $\beta$ -hydroxydeoxyisoaustamide (7), which was previously isolated from this strain. This was additionally proven through comparison of experimental MS/MS spectra and RT with an in-house database (Figure S36). One more closely related alkaloid austamide (13) with the same molecular formula was identified for the peak at 5.2 min with  $m/z$  364.1654 using the GNPS database.

The peak detected at 7.6 min with  $m/z$  350.1870 corresponded to the molecular formula  $C_{21}H_{23}N_3O_2$ , the same as deoxydihydroisoaustamide (10), which was previously isolated from this strain [8]. This was additionally proven through comparison of experimental MS/MS spectra and RT with an in-house database (Figure S38).

The peak detected at 10.8 min with  $m/z$  346.1562 corresponded to the molecular formula  $C_{21}H_{19}N_3O_2$ , the same as deoxy-14,15-dehydroisoaustamide (8), which was previously isolated from this strain [9]. Unfortunately, we did not have a reference compound to obtain MS/MS data and retention times to uniquely identify this compound.

The peak detected at 7.3 min with  $m/z$  396.194 corresponded to the molecular formula  $C_{22}H_{25}N_3O_4$ , which can be associated with three stereoisomeric alkaloids previously isolated from this strain: 16 $\alpha$ -hydroxy-17 $\beta$ -methoxy-deoxydihydroisoaustamide (1), 16 $\beta$ -hydroxy-17 $\alpha$ -methoxy-deoxydihydroisoaustamide (2) and 16 $\alpha$ -hydroxy-17 $\alpha$ -methoxy-deoxydihydroisoaustamide (3). This was additionally proven through comparison of experimental MS/MS spectra and RT with an in-house database (Figures S30–S32). The RT of reference compounds were very close; therefore, all three compounds can be contained in one peak of the extract HPLC MS chromatograms.

The peaks detected at 6.0 and 6.6 min with  $m/z$  396.194 corresponded to the molecular formula  $C_{21}H_{23}N_3O_4$ , which can be associated with the stereoisomeric alkaloids previously isolated from this strain 16,17-dihydroxy-deoxydihydroisoaustamide (4), 16 $\beta$ ,17 $\alpha$ -dihydroxy-deoxydihydroisoaustamide (5) and 16 $\alpha$ ,17 $\alpha$ -dihydroxy-deoxydihydroisoaustamide (6). The comparison of experimental MS/MS spectra and RT with the values obtained for reference compounds showed that RT 6.0 and 6.6 min correspond to 16 $\beta$ ,17 $\alpha$ -dihydroxy-deoxydihydroisoaustamide (5) and 16 $\alpha$ ,17 $\alpha$ -dihydroxy-deoxydihydroisoaustamide (6) (Figures S34 and S35). The peak detected at 6.2 min with same  $m/z$  likely corresponds to 16,17-dihydroxy-deoxydihydroisoaustamide (4) (Figure S33), but this peak was only detected in extracts in trace quantities and we have no MS/MS for exact identification.

The peak detected at 9.6 min ( $m/z$  352.2010) corresponded to the molecular formula  $C_{21}H_{23}N_3O_2$ , which can be associated with the desoxybrevianamide E (11) previously isolated from this strain. This was additionally proven through comparison of experimental MS/MS spectra and RT with an in-house database (Figure S39).

The peak detected at 5.0 min ( $m/z$  284.1386) corresponded to the molecular formula  $C_{16}H_{17}N_3O_2$  and was associated with the known brevianamide F (12) using the GNPS database.

The peaks detected at 13.0 ( $m/z$  271.0597), 8.7 ( $m/z$  287.0545), 10.1 ( $m/z$  321.0160) and 8.1 ( $m/z$  315.0490) min corresponded to the molecular formulas  $C_{15}H_{10}O_5$ ,  $C_{15}H_{10}O_6$ ,  $C_{15}H_9ClO_6$  and  $C_{16}H_{10}O_7$ , and were associated with anthraquinone derivatives emodine (13) [23], citreorsein (15) [24], 2-chlorocitreorsein (16) [25] and endocrocin (17) [26], respectively, using the GNPS database.

The peaks detected at 15.5 ( $m/z$  579.0609) and 15.7 ( $m/z$  579.0614) min corresponded to the molecular formulas  $C_{30}H_{20}Cl_2O_8$ , and were associated with the stereoisomeric bisanthrone derivatives nephrolaevigatins A (18) and B (19), respectively, using the GNPS database [27]. The peaks detected at 15.3 ( $m/z$  545.1005) and 15.0 ( $m/z$  545.1012) min corresponded to the molecular formulas  $C_{30}H_{21}ClO_8$ , and were associated with the stereoisomeric bisanthrone derivatives nephrolaevigatins C (20) and D (21), respectively, using the GNPS database [27]. It should be noted that the identification of compounds 18–21 was

carried out not only on the basis of the identity of the MS/MS spectra, but also based on the correspondence of the RT, which made it possible to identify specific stereoisomers [27].

The peaks detected at 13.6 ( $m/z$  639.1747), 4.9 ( $m/z$  209.081) and 5.1 ( $m/z$  235.096) min corresponded to the molecular formulas  $C_{32}H_{30}O_{14}$ ,  $C_{11}H_{12}O_4$  and  $C_{13}H_{14}O_4$ , and were associated with secalonic acid D (**22**) [28], cinnamic acid (**23**) and isochromen (**24**) derivatives, respectively, using the GNPS database. The peak detected at 19.9 min with  $m/z$  411.324 corresponded to the molecular formula  $C_{28}H_{42}O_2$ , and can be associated with the unidentified ergostane derivative (**25**) according to characteristic MS/MS spectra.

The use of FBMN together with the in-house database made it possible to reveal several clusters of related features, the largest of which was assigned to brevianamide alkaloids and contained not only identified compounds **5–13**, but also a few unidentified compounds (Figure 5).

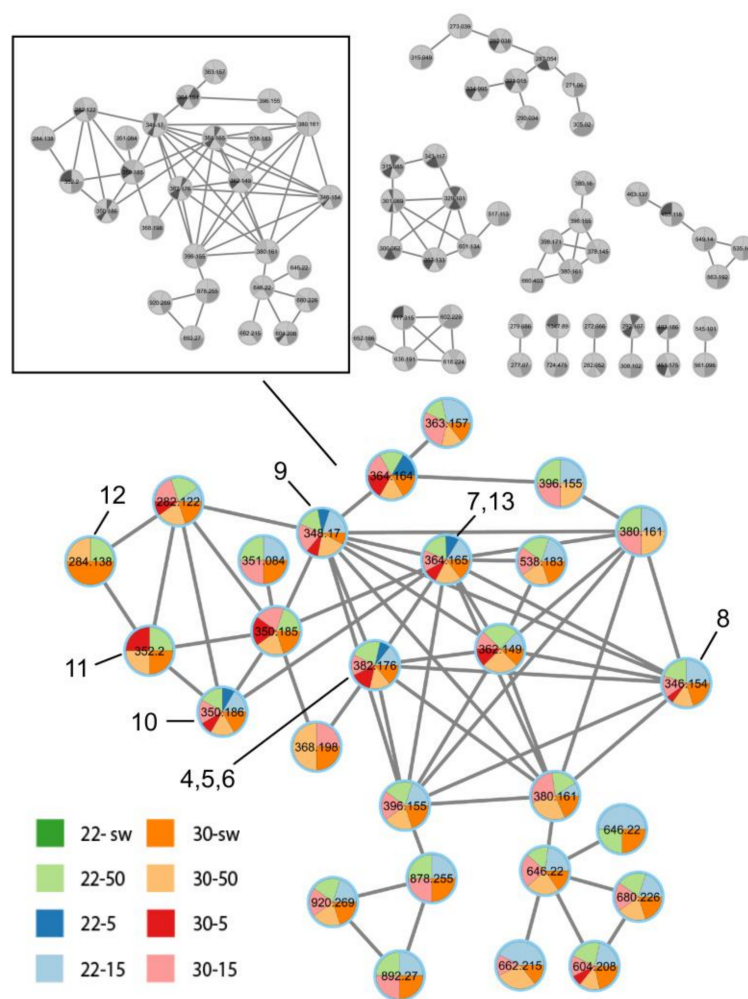


**Figure 5.** Feature-based molecular network (FBMN) of the extracts of strain KMM 4689. The cluster containing library hits for brevianamide-related alkaloids is highlighted. Feature identity is annotated with the results from the in-house library identification (**4–11**) and the GNPS identification (**12** and **13**). The precursor mass of all identified alkaloids corresponds to the  $[M+H]^+$  adduct of these alkaloids. A pie chart shows the distribution of the metabolite extract according to the legend.

The relative content of the compounds in the studied extracts was calculated as a percentage of the total area of the corresponding peaks in the HPLC MS chromatograms and is presented as a heatmap (Figure 6). A main compound detected in all extracts was (+)-deoxyisoaustamide (**9**), the amount of which was increased in hypo- and hypersalinity cultures, excluding the 22-5 extract.  $3\beta$ -hydroxydeoxyisoaustamide (**7**) and deoxydihy-

droisoaustamide (10) were also detected as major compounds, and their amounts were decreased in extracts obtained with 5 µg/mL of sea salt. The neuroprotective alkaloids 5 and 6 were detected in the greatest amount in the extract obtained after culture at 30 °C and with hypersalinity. Other alkaloids (1–3, 11–13) were found only in small amounts, and compounds 12 and 13 were not detected at all in extract 30-5.

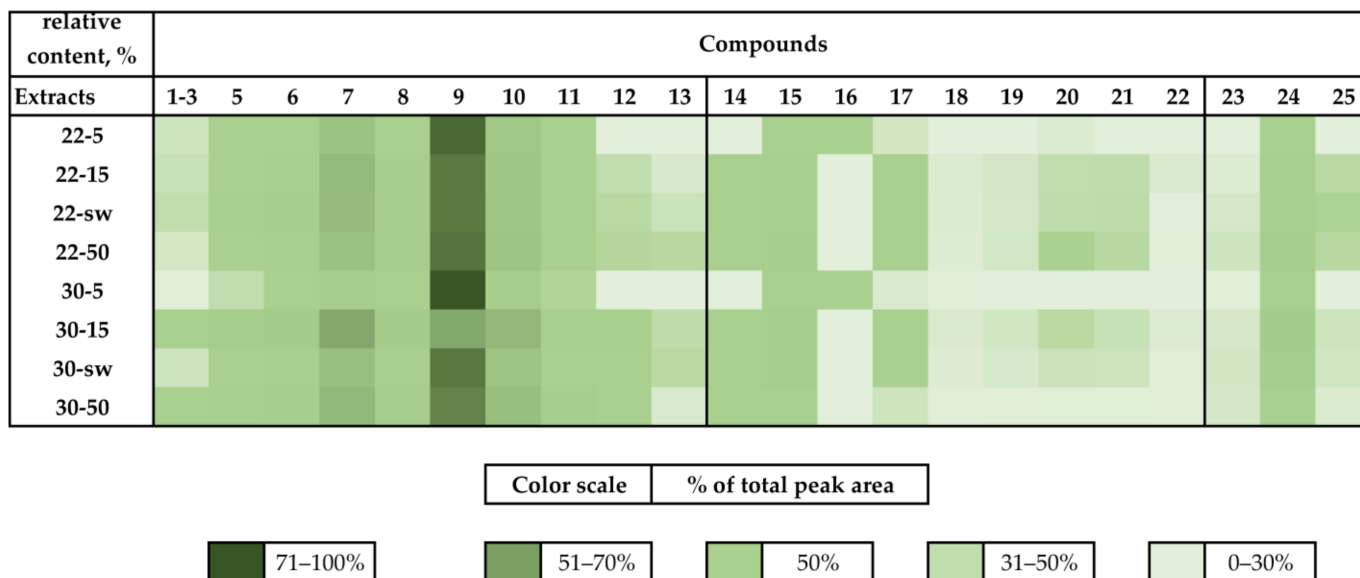


**Figure 6.** The heat map of a relative content of compounds 1–25 identified in fungal extracts. Each cell presents data about percentage of compound peak area to total area of peaks in extract.

Under hyposaline conditions (22-5 and 30-5), the content of almost all anthraquinone pigments sharply decreased, with the exception of 2-chlorocitreorosein (16), which was found only in these extracts (Figure 6). In addition, the content of bisanthrone derivatives 18–21 decreased with an increase in cultivation temperature to 30 °C. Interestingly, the relative content of citreorosein (15) and isochromene derivative (24) was stable in all extracts. The change in the content of the cinnamic acid derivative (23) occurred in direct proportion to the change in the salt content in the medium, regardless of cultivation temperature. The content of ergostane triterpenoid (25) hardly changed at 22 °C, except for a decrease in hyposaline conditions (22-5), and decreased with any deviation from the natural content of sea salt at 30 °C.

Overall, hyposaline conditions (especially at a lower temperature) of cultivation significantly reduced the content of almost all detected compounds. Hyper salinity caused a change in metabolism, which was expressed in an increase or decrease in the content of individual detected metabolites.

Principal component analysis (PCA) was used to distinguish between extracts that were analyzed using HPLC MS. The PCA model showed an optimal number of principal components (PCs) equal to two, so two PCs (PC1 and PC2) were chosen to describe ≈99% of the variations in the samples. The first principal component describes about 92% of variance and the second principal component describes ≈7% of variations (Figure 7).

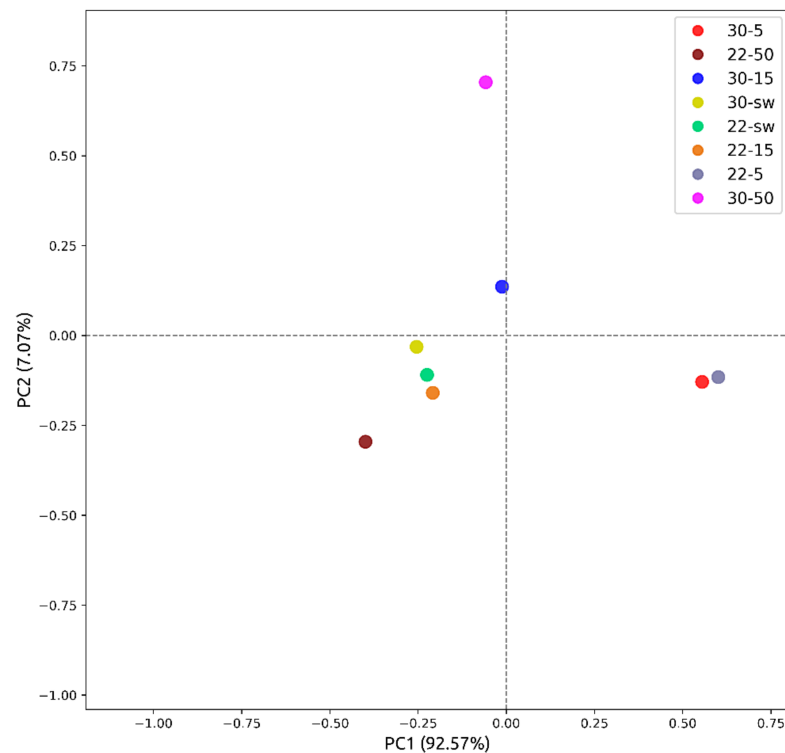


**Figure 7.** The principal component analysis (PCA) of various fungal extracts.

The results of the PCA analysis showed that the extracts obtained during cultivation with standard salinity, regardless of temperature (22-sw and 30-sw), are close to each other in the two principal components. Extract 22-15 is also close to this group. The extracts obtained after hyposaline cultivation (22-5 and 30-5) have large differences from the first group of samples according to PC1. Extracts 30-50 and 30-15 are different from each other in PC2 and are different from the first group of extracts in PC1. Extract 22-50 differs from the first group of extracts and other groups in both PC1 and PC2.

### 3.2. Molecular Re-Identification of the Fungal Strain

The study of secondary metabolites of the strain KMM 4689 showed that although brevianamide-related alkaloids and anthraquinone pigments are widely distributed in various fungi, these metabolites have not yet been described for *P. dimorphosporum* and related species. For this reason, the KMM 4689 strain was re-sequenced using a combination of two molecular markers (ITS and  $\beta$ -tubulin regions).

Approximately 1200 bp fragments of the ITS gene region and 450 bp fragments of the  $\beta$ -tubulin gene were successfully amplified. BLAST search results indicated that the sequences were 99.52–100% identical to the sequences of the ex-type strain *Penicillium hispanicum* CBS 691.77. The phylogenetic ML tree constructed on the basis of the concatenated ITS gene and partial  $\beta$ -tubulin gene sequences clearly showed that the strain KMM 4689 belongs to the *Ramigena* seria of *Ramigena* section together with *Penicillium capsulatum*, *P. cyaneum*, *P. ornatum* and *P. ramusculum* (Figure 8). The phylogenetic ML tree of ITS region sequences showing the phylogenetic position of the strain KMM 4689 among members of the genus *Penicillium* section *Ramigena* and section *Exilicaulis* (*P. dimorphosporum*) is presented in Figure S29.

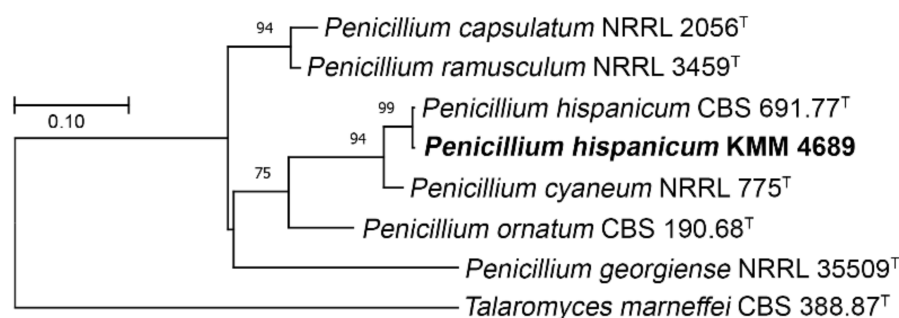


**Figure 8.** ML tree based on concatenated ITS region and partial  $\beta$ -tubulin gene sequences showing phylogenetic position of the strain KMM 4689 among members of genus *Penicillium* section *Ramigena*. Bootstrap values (%) of 1000 replications. Nodes with confidence values greater than 50% are indicated. The scale bar represents 0.1 substitutions per site.

#### 4. Discussion

The fungal strain KMM 4689 was originally identified as *P. dimorphosporum* according to morphological features, ITS molecular data and its association with the marine environment [8]. *P. dimorphosporum* was firstly isolated from mangrove swamp soil (Australia) and described by H.J. Swart in 1970 [29]. ITS is a widely used sequence marker for fungi, but its data give good results for identifications at the complex or section level. Because of some limitations associated with ITS as a species-level marker, we used the  $\beta$ -tubulin gene as a secondary identification marker [30]. Re-identification was based on the concatenated ITS gene and partial  $\beta$ -tubulin gene sequences showing the phylogenetic position of the strain KMM 4689 among members of the genus *Penicillium* section *Ramigena* (Figures 8 and S29).

Both *P. dimorphosporum* and *P. hispanicum* share some similarities such as slow growth on CYA, monoverticillate conidiophores and pigment production. However, the secondary metabolites reported from these fungi to date are quite different.

*P. dimorphosporum* fungus belongs to the *Exilicaulis* section of the *Erubescens* series (Figure S29). This series includes 16 species with restricted colony, short monoverticillate conidiophores and conidia with variable shapes [31]. The fungi of the *Exilicaulis* section are characterized by the production of long-chain polyketides [32–34], benzopyrans [35], chromones and xanthenes [36], as well as the simplest dipeptides, non-prenylated indole and diketopiperazine alkaloids [37].

*P. hispanicum* is in the *Ramigena* section of the *Ramigena* series together with *Penicillium capsulatum*, *P. cyaneum*, *P. ornatum* and *P. ramusculum* [31]. The metabolism of these fungi is relatively poorly understood. To date, they have been described as producers of anthraquinone and bisanthrone pigments [31], and a number of other polyketides [38,39]. Moreover, *P. hispanicum* was reported as a source of brevianamide-related alkaloid desoxybrevianamide E (**11**) [31], which was identified by us in all studied fungal extracts and which is the precursor of related compounds **1–10** and **13**. The identification of brevianamide F (**12**) allowed us to suggest the biosynthesis scheme of the 2,5-diketopiperazine alkaloids in this fungal strain (Figure 9).

The change in fungal culture conditions induced a change in the metabolite profiles of the fungal extracts detected through both HPLC UV and HPLC MS approaches, indicating a significant influence of culture conditions on the metabolism of this fungus.

Comparison of the number of peaks in HPLC UV chromatograms both at 220 nm and at 290 nm detection as well as peak areas with the masses of purified extracts showed no direct relationships. The extracts of cultures obtained under hyposaline conditions (22-5 and 30-5) have the largest masses of extracts but a minimal area of peaks in the HPLC UV chromatograms. The increase in cultivation temperature to 30 °C did not result in a change in extract masses, but induced an increase in the area of peaks in the polar and middle polar zones of the HPLC UV chromatograms at 220 nm.

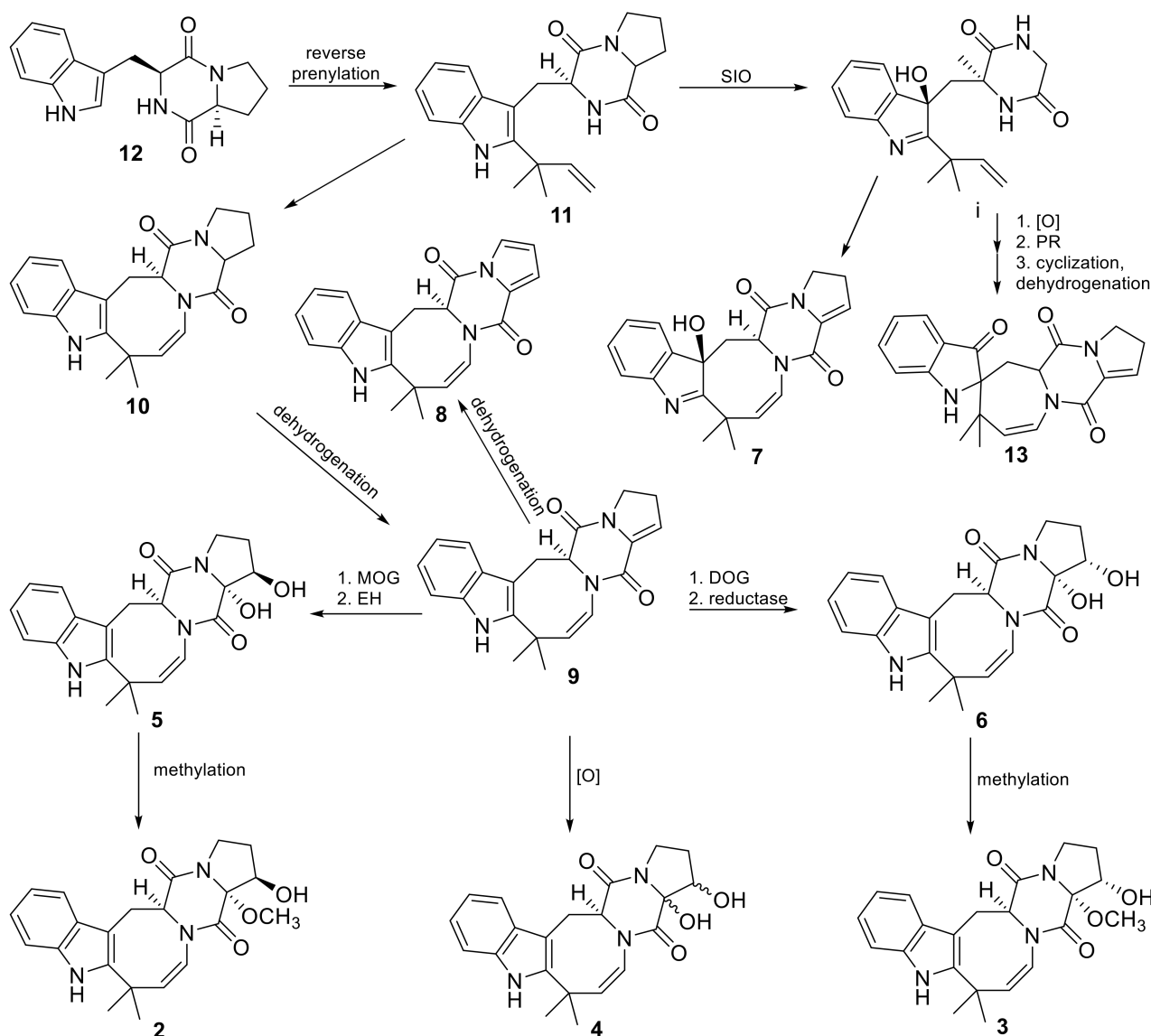


**Figure 9.** Plausible biosynthetic pathway for alkaloids 1–13 in *Penicillium hispanicum*. SIO—R-selective indoloxidase, PR—pinacol rearrangement, DOG—dioxygenase, MOG—monooxygenase, EH—epoxide hydrolase.

HPLC MS detection allowed us to identify 25 compounds, but only 14 compounds, 1–11, 15, 17 and 24, were identified in all studied extracts. Compounds 12 and 13 as well as 14, 19, 21, 22, and 25 were not identified in the 22-5 and 30-5 extracts. Compounds 18 and 23 were not identified in extract 22-5. Compound 20 was not identified in the 30-5 extract. 2-Chlorocitreosein (16) was identified only in the 22-5 and 30-5 extracts. Therefore, strong hyposalinity conditions clearly have the most significant influence on the metabolite profile of this fungal strain. In addition, about 20 visible HPLC MS peaks were not identified and yet more differences in the metabolite profiles of extracts can be discovered in this field.

All studied extracts shown a moderate DPPH activity, and this effect was observed to be high for extracts 22-5 and 22-50 as well as 30-5. The alkaloids 1–13 did not show DPPH radical scavenging. Anthraquinone derivatives 14–21 also could not be described as radical scavengers [40]. Cinnamic acid derivative 23 showed weak DPPH radical scavenging activity [41]. No antioxidant activity for isochromene derivative 24 was reported, but other isochromenes demonstrated earlier DPPH radical scavenging effect [42]. Therefore, the high DPPH radical scavenging activity of several extracts may be considered with unidentified compounds.

The moderate cytotoxicity of extracts may be caused by a presence of compounds 13 [43], 14 [44], 16 [45] and 22 [46]. The most cytotoxic extract 22-50 contained the maximum amount of the most-detected metabolites, which probably explains its cytotoxicity, while extract 22-5, characterized by a low content of many identified compounds, also showed the weakest cytotoxic activity. On the other hand, the extracts can contain other cytotoxic compounds.

Therefore, the production of known neuroprotective alkaloids 5, 6 and other brevianamide alkaloids was increased in hypersaline and high-temperature conditions, and this may be an adaptation to extreme conditions. On the other hand, hyposalinity stress may induce the synthesis of unidentified antioxidants with low cytotoxicity that could be very interesting for future investigation.

## 5. Conclusions

In total, 25 varying compounds including 13 desoxyisoaustamide alkaloids and eight anthraquinones were identified in different combinations in the extracts, obtained after changes in the fungal strain KMM 4689 cultivation conditions, and the relative amounts of identified metabolites were estimated. The production of known neuroprotective alkaloids 16,17-dihydroxy-deoxydihydroisoaustamides (4–6) and other brevianamide alkaloids was increased in hypersaline and high-temperature conditions, and this may be an adaptation to extreme conditions. On the other hand, the hyposalinity stress may induce the synthesis of unidentified antioxidants with low cytotoxicity that could be very interesting for future investigation.

The study of secondary metabolites of the strain KMM 4689 showed that although brevianamide-related alkaloids and anthraquinone pigments are widely distributed in various fungi, these metabolites have not been described for *Penicillium dimorphosporum* and related species. For this reason, the strain KMM 4689 was re-identified as *P. hispanicum* using a combination of the ITS region and  $\beta$ -tubulin gene sequences as molecular markers.

**Supplementary Materials:** The following supporting information can be downloaded at: <https://www.mdpi.com/article/10.3390/fermentation9040337/s1>, Figures S1–S20: HPLC UV chromatograms for all analyzed extracts; Figures S21–S28: UHPLC MS chromatograms for extracts 22-sw, 22-5, 22-15, 22-50, 30-sw, 30-5, 30-15, 30-50; Figure S29: ITS gene-based ML tree for *P. hispanicum* and *P. dimorphosporum*; Figures S30–S39: HPLC MS chromatograms for reference compounds 1–10.

**Author Contributions:** Conceptualization, E.A.Y. and A.N.Y.; Data curation, R.S.P.; Formal analysis, N.N.K., V.E.C., E.A.Y. and A.N.Y.; Funding acquisition, M.P.I.; Investigation, L.E.N., R.S.P., O.I.Z., N.N.K., V.E.C., K.S.K., M.V.P. and E.A.Y.; Project administration, M.P.I.; Resources, A.N.Y.; Supervision, M.P.I. and A.N.Y.; Validation, R.S.P., O.I.Z., E.A.Y., M.P.I. and A.N.Y.; Visualization, L.E.N., N.N.K., V.E.C., K.S.K., E.A.Y. and A.N.Y.; Writing—original draft, L.E.N., N.N.K., V.E.C. and E.A.Y.; Writing—review and editing, M.P.I. and A.N.Y. All authors have read and agreed to the published version of the manuscript.

**Funding:** This research was funded by a grant from the Ministry of Science and Higher Education of the Russian Federation 15.BRK.21.0004 (Contract No. 075-15-2021-1052).

**Institutional Review Board Statement:** Not applicable.

**Informed Consent Statement:** Not applicable.

**Data Availability Statement:** The FBMN is available from the GNPS website through the following link: <https://gnps.ucsd.edu/ProteoSAFe/status.jsp?task=edcc91ae9f2943ac8a3bd2ad4e94ae10> (accessed on 28 October 2022).

**Acknowledgments:** We are grateful to Sergey Baldaev for Sanger sequencing of nucleotide sequences. The study was carried out using the Collective Facilities Center “Collection of Marine Microorganisms PIBOC FEB RAS” and on the equipment of the Collective Facilities Center, “The Far Eastern Center for Structural Molecular Research (NMR/MS) PIBOC FEB RAS”.

**Conflicts of Interest:** The authors declare no conflict of interest.

## Appendix A

Table A1. The identified compounds.

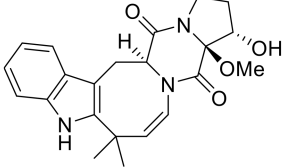
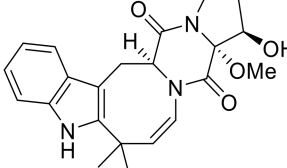
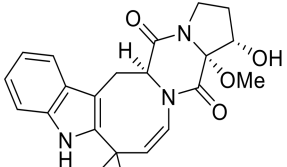
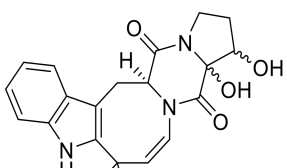
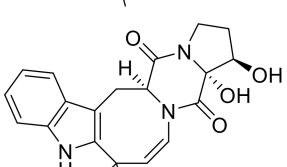
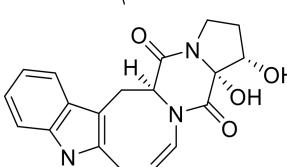
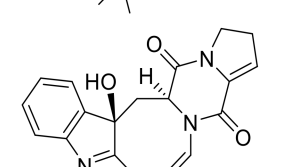
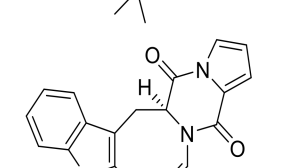
N	Name	Structure	RT	Exact Mass (Measured)	Exact Mass (Calcd)	$\Delta$ , ppm	MQScore (GNPS)	Ref.
1	16 $\alpha$ -hydroxy-17 $\beta$ -methoxy-deoxydihydroisoaustamide		7.3	396.194 [M+H] <sup>+</sup>	396.1918	−5.6	*	[8]
2	16 $\beta$ -hydroxy-17 $\alpha$ -methoxy-deoxydihydroisoaustamide		7.3	396.194 [M+H] <sup>+</sup>	396.1918	−5.6	*	[8]
3	16 $\alpha$ -hydroxy-17 $\alpha$ -methoxy-deoxydihydroisoaustamide		7.3	396.194 [M+H] <sup>+</sup>	396.1918	−5.6	*	[8]
4	16,17-dihydroxy-deoxydihydroisoaustamide		6.2	382.176 [M+H] <sup>+</sup>	382.1761	0.3	*	[8]
5	16 $\beta$ ,17 $\alpha$ -dihydroxy-deoxydihydroisoaustamide		6.0	382.176 [M+H] <sup>+</sup>	382.1761	0.3	*	[8]
6	16 $\alpha$ ,17 $\alpha$ -dihydroxy-deoxydihydroisoaustamide		6.6	382.176 [M+H] <sup>+</sup>	382.1761	0.3	*	[8]
7	3 $\beta$ -hydroxydeoxyisoaustamide		2.9	364.1645 [M+H] <sup>+</sup>	364.1656	3.0	*	[8]
8	deoxy-14,15-dehydroisoaustamide		10.8	346.1562 [M+H] <sup>+</sup>	346.1550	3.4	**	[9]

Table A1. Cont.

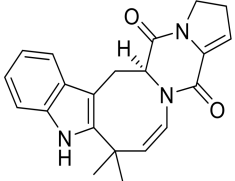
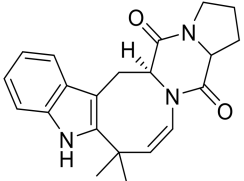
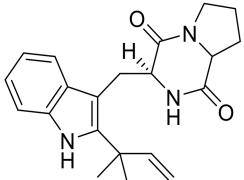
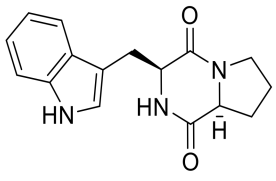
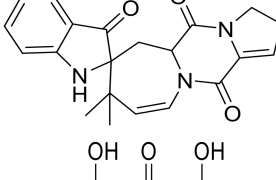
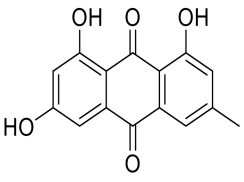
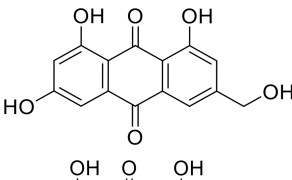
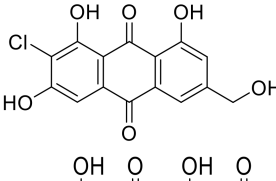
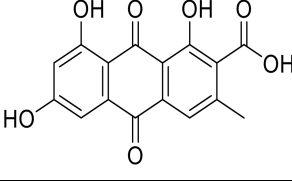
N	Name	Structure	RT	Exact Mass (Measured)	Exact Mass (Calcd)	$\Delta$ , ppm	MQScore (GNPS)	Ref.
9	(+)-deoxyisoaustamide		7.7	348.1697 [M+H] <sup>+</sup>	348.1707	2.9	*	[8]
10	deoxydihydroisoaustamide		7.6	350.1870 [M+H] <sup>+</sup>	350.1863	-2.0	*	[8]
11	desoxybrevianamide E		9.7	352.2010 [M+H] <sup>+</sup>	352.2020	2.7	*	[8]
12	brevianamide F		5.0	284.1386 [M+H] <sup>+</sup>	284.1394	2.7	0.98	[47]
13	austamide		5.2	364.1654 [M+H] <sup>+</sup>	364.1656	0.5	0.81	[43]
14	emodine		13.0	271.0597 [M+H] <sup>+</sup>	271.0601	1.5	0.94	[14, 48]
15	citreorosein		8.7	287.0545 [M+H] <sup>+</sup>	287.0550	1.8	0.89	[14, 49]
16	2-chlorocitreorosein		10.1	321.016 [M+H] <sup>+</sup>	321.0160	0.1	0.86	[25]
17	endocrocin		8.1	315.0490 [M+H] <sup>+</sup>	315.0499	2.9	0.96	[14]

Table A1. Cont.

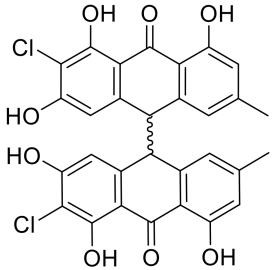
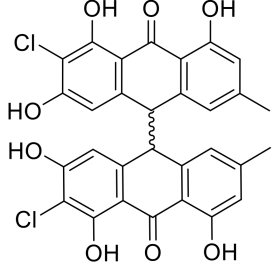
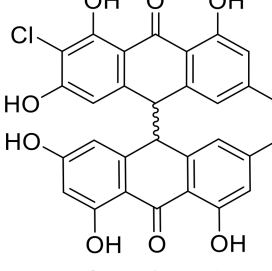
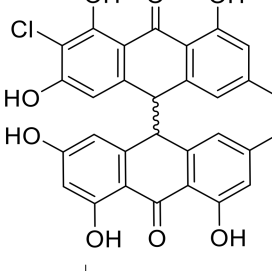
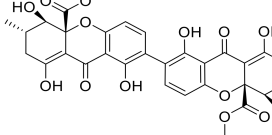
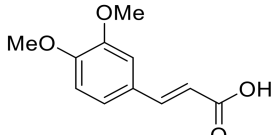
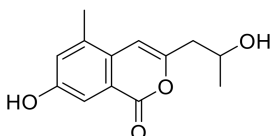
N	Name	Structure	RT	Exact Mass (Measured)	Exact Mass (Calcd)	$\Delta$ , ppm	MQScore (GNPS)	Ref.
18	nephrolaevigatin A		15.5	579.0609 [M+H] <sup>+</sup>	579.0608	−0.2	0.81	[27]
19	nephrolaevigatin B		15.7	579.0614 [M+H] <sup>+</sup>	579.0608	−1.04	0.81	[27]
20	nephrolaevigatin C		15.3	545.1005 [M+H] <sup>+</sup>	545.0998	−1.3	0.89	[27]
21	nephrolaevigatin D		15.0	545.1012 [M+H] <sup>+</sup>	545.0998	−2.6	0.89	[27]
22	secalonic acid D		13.6	639.1747 [M+H] <sup>+</sup>	639.1708	−6.1	0.82	[50, 51]
23	3,4-dimethoxycinnamic acid		4.9	209.081 [M+H] <sup>+</sup>	209.0804	−0.8	0.90	[52]
24	7-hydroxy-3-(2-hydroxypropyl)-5-methylisochromen-1-one		5.1	235.096 [M+H] <sup>+</sup>	235.0965	2.1	0.86	[53]

Table A1. Cont.

N	Name	Structure	RT	Exact Mass (Measured)	Exact Mass (Calcd)	$\Delta$ , ppm	MQScore (GNPS)	Ref.
25	unidentified ergostane derivative	C <sub>28</sub> H <sub>42</sub> O <sub>2</sub>	19.9	411.324 [M+H] <sup>+</sup>	411.3258	4.3		

\* Compounds were identified through comparison of MS/MS data and retention time with those obtained for authentic standards previously isolated from this fungal strain [8]. \*\* Compound was identified based on an exact mass value.

## References

- Dewapriya, P.; Kim, S.K. Marine microorganisms: An emerging avenue in modern nutraceuticals and functional foods. *Food Res. Int.* **2014**, *56*, 115–125. [\[CrossRef\]](#)
- Takahashi, J.A.; Barbosa, B.V.R.; Martins, B.A.; Guirlanda, C.P.; Moura, M.A.F. Use of the versatility of fungal metabolism to meet modern demands for healthy aging, functional foods, and sustainability. *J. Fungi* **2020**, *6*, 223. [\[CrossRef\]](#) [\[PubMed\]](#)
- Pinedo-Rivilla, C.; Aleu, J.; Durán-Patrón, R. Cryptic Metabolites from Marine-Derived Microorganisms Using OSMAC and Epigenetic Approaches. *Mar. Drugs* **2022**, *20*, 84. [\[CrossRef\]](#)
- Bode, H.B.; Bethe, B.; Höfs, R.; Zeeck, A. Big effects from small changes: Possible ways to explore nature's chemical diversity. *ChemBioChem* **2002**, *3*, 619–627. [\[CrossRef\]](#)
- Petersen, L.E.; Marnier, M.; Labes, A.; Tasdemir, D. Rapid metabolome and bioactivity profiling of fungi associated with the leaf and rhizosphere of the baltic seagrass *zostera marina*. *Mar. Drugs* **2019**, *17*, 419. [\[CrossRef\]](#) [\[PubMed\]](#)
- Overy, D.; Correa, H.; Roullier, C.; Chi, W.C.; Pang, K.L.; Rateb, M.; Ebel, R.; Shang, Z.; Capon, R.; Bills, G.; et al. Does Osmotic Stress Affect Natural Product Expression in Fungi? *Mar. Drugs* **2017**, *15*, 254. [\[CrossRef\]](#) [\[PubMed\]](#)
- Igboeli, H.A.; Marchbank, D.H.; Correa, H.; Overy, D.; Kerr, R.G. Discovery of Primarolides A and B from Marine Fungus *Asteromyces cruciatus* Using Osmotic Stress and Treatment with Suberoylanilide Hydroxamic Acid. *Mar. Drugs* **2019**, *17*, 435. [\[CrossRef\]](#)
- Zhuravleva, O.I.; Antonov, A.S.; Trang, V.T.D.; Pivkin, M.V.; Khudyakova, Y.V.; Denisenko, V.A.; Popov, R.S.; Kim, N.Y.; Yurchenko, E.A.; Gerasimenko, A.V.; et al. New Deoxyisoaustamide Derivatives from the Coral-Derived Fungus *Penicillium dimorphosporum* KMM 4689. *Mar. Drugs* **2021**, *19*, 32. [\[CrossRef\]](#)
- Dyshlovoy, S.A.; Zhuravleva, O.I.; Hauschild, J.; Busenbender, T.; Pelageev, D.N.; Yurchenko, A.N.; Khudyakova, Y.V.; Antonov, A.S.; Graefen, M.; Bokemeyer, C.; et al. New Marine Fungal Deoxy-14,15-Dehydroisoaustamide Resensitizes Prostate Cancer Cells to Enzalutamide. *Mar. Drugs* **2023**, *21*, 54. [\[CrossRef\]](#)
- Chambers, M.C.; MacLean, B.; Burke, R.; Amodei, D.; Ruderman, D.L.; Neumann, S.; Gatto, L.; Fischer, B.; Pratt, B.; Egertson, J.; et al. A cross-platform toolkit for mass spectrometry and proteomics. *Nat. Biotechnol.* **2012**, *30*, 918–920. [\[CrossRef\]](#)
- Pluskal, T.; Castillo, S.; Villar-Briones, A.; Orešič, M. MZmine 2: Modular framework for processing, visualizing, and analyzing mass spectrometry-based molecular profile data. *BMC Bioinform.* **2010**, *11*, 395. [\[CrossRef\]](#)
- Myers, O.D.; Sumner, S.J.; Li, S.; Barnes, S.; Du, X. One Step Forward for Reducing False Positive and False Negative Compound Identifications from Mass Spectrometry Metabolomics Data: New Algorithms for Constructing Extracted Ion Chromatograms and Detecting Chromatographic Peaks. *Anal. Chem.* **2017**, *89*, 8696–8703. [\[CrossRef\]](#) [\[PubMed\]](#)
- Nothias, L.F.; Petras, D.; Schmid, R.; Dührkop, K.; Rainer, J.; Sarvepalli, A.; Protsyuk, I.; Ernst, M.; Tsugawa, H.; Fleischauer, M.; et al. Feature-based molecular networking in the GNPS analysis environment. *Nat. Methods* **2020**, *17*, 905–908. [\[CrossRef\]](#) [\[PubMed\]](#)
- Christiansen, J.V.; Larsen, T.O.; Frisvad, J.C. Production of Fungal Quinones: Problems and Prospects. *Biomolecules* **2022**, *12*, 1041. [\[CrossRef\]](#)
- Aron, A.T.; Gentry, E.C.; McPhail, K.L.; Nothias, L.F.; Nothias-Esposito, M.; Bouslimani, A.; Petras, D.; Gauglitz, J.M.; Sikora, N.; Vargas, F.; et al. Reproducible molecular networking of untargeted mass spectrometry data using GNPS. *Nat. Protoc.* **2020**, *15*, 1954–1991. [\[CrossRef\]](#) [\[PubMed\]](#)
- Pedregosa, F.; Varoquaux, G.; Gramfort, A.; Michel, V.; Thirion, B.; Grisel, O.; Blondel, M.; Prettenhofer, P.; Weiss, R.; Dubourg, V.; et al. Scikit-learn: Machine learning in Python. *J. Mach. Learn. Res.* **2011**, *12*, 2825–2830. [\[CrossRef\]](#)
- Bedre, R. *Reneshbedre/Bioinfokit: Bioinformatics Data Analysis and Visualization Toolkit, 2.0.9*, Zenodo, 2022.
- Scholin, C.A.; Herzog, M.; Sogin, M.; Anderson, D.M. Identification of group- and strain-specific genetic markers for globally distributed *Alexandrium* (*Dinophyceae*). II. Sequence analysis of a fragment of the LSU rRNA gene. *J. Phycol.* **1994**, *30*, 999–1011. [\[CrossRef\]](#)
- Elwood, H.J.; Olsen, G.J.; Sogin, M.L. The small-subunit ribosomal RNA gene sequences from the hypotrichous ciliates *Oxytricha nova* and *Stylonychia pustulata*. *Mol. Biol. Evol.* **1985**, *2*, 399–410. [\[PubMed\]](#)
- Glass, N.L.; Donaldson, G.C. Development of primer sets designed for use with the PCR to amplify conserved genes from filamentous ascomycetes. *Appl. Environ. Microbiol.* **1995**, *61*, 1323–1330. [\[CrossRef\]](#)
- Kumar, S.; Stecher, G.; Li, M.; Niyaz, C.; Tamura, K. MEGA X: Molecular evolutionary genetics analysis across computing platforms. *Mol. Biol. Evol.* **2018**, *35*, 1547. [\[CrossRef\]](#)

22. Tamura, K.; Nei, M. Estimation of the number of nucleotide substitutions in the control region of mitochondrial DNA in humans and chimpanzees. *Mol. Biol. Evol.* **1993**, *10*, 512–526.
23. Monisha, B.A.; Kumar, N.; Tiku, A.B. Emodin and its role in chronic diseases. *Adv. Exp. Med. Biol.* **2016**, *928*, 47–73. [[PubMed](#)]
24. Graf, T.N.; Kao, D.; Rivera-Chávez, J.; Gallagher, J.M.; Raja, H.A.; Oberlies, N.H. Drug leads from endophytic fungi: Lessons learned via scaled production. *Planta. Med.* **2020**, *86*, 988–996. [[CrossRef](#)] [[PubMed](#)]
25. Yamamoto, Y.; Kiriya, N.; Arahata, S. Studies on the Metabolic Products of *Aspergillus fumigatus* (J-4). Chemical Structure of Metabolic Products. *Chem. Pharm. Bull.* **1968**, *16*, 304–310. [[CrossRef](#)] [[PubMed](#)]
26. Kurobane, I.; Vining, L.C.; Gavin McInnes, A. Biosynthetic relationships among the secalonic acids isolation of emodin, endocrocin and secalonic acids from *pyrenochaeta terrestris* and *aspergillus aculeatus*. *J. Antibiot.* **1979**, *32*, 1256–1266. [[CrossRef](#)]
27. Lagarde, A.; Mambu, L.; Mai, P.Y.; Champavier, Y.; Stigliani, J.L.; Beniddir, M.A.; Millot, M. Chlorinated bianthrone from the cyanolichen *Nephroma laevigatum*. *Fitoterapia* **2021**, *149*, 104811. [[CrossRef](#)]
28. Wang, B.H.; Polya, G.M. The fungal teratogen secalonic acid D is an inhibitor of protein kinase C and of cyclic AMP-dependent protein kinase. *Planta. Med.* **1996**, *62*, 111–114. [[CrossRef](#)] [[PubMed](#)]
29. Swart, H.J. *Penicillium dimorphosporum* sp. nov. *Trans. Br. Mycol. Soc.* **1970**, *55*, 310–313. [[CrossRef](#)]
30. Visagie, C.M.; Houbraken, J.; Frisvad, J.C.; Hong, S.B.; Klaassen, C.H.W.; Perrone, G.; Seifert, K.A.; Varga, J.; Yaguchi, T.; Samson, R.A. Identification and nomenclature of the genus *Penicillium*. *Stud. Mycol.* **2014**, *78*, 343–371. [[CrossRef](#)]
31. Houbraken, J.; Kocsube, S.; Visagie, C.M.; Yilmaz, N.; Wang, X.C.; Meijer, M.; Kraak, B.; Hubka, V.; Bensch, K.; Samson, R.A.; et al. Classification of *Aspergillus*, *Penicillium*, *Talaromyces* and related genera (*Eurotiales*): An overview of families, genera, subgenera, sections, series and species. *Stud. Mycol.* **2020**, *95*, 5–169. [[CrossRef](#)]
32. Hensens, O.D.; Wichmann, C.F.; Liesch, J.M.; Vanmiddlesworth, F.L.; Wilson, K.E.; Schwartz, R.E. Structure elucidation of restricticin, a novel antifungal agent from *Penicillium restrictum*. *Tetrahedron* **1991**, *47*, 3915–3924. [[CrossRef](#)]
33. Brill, G.M.; Chen, R.H.; Rasmussen, R.R.; Whittern, D.N.; McAlpine, J.B. Calbistrins, novel antifungal agents produced by *Penicillium restrictum*. 2. Isolation and elucidation of structure. *J. Antibiot.* **1993**, *46*, 39–47. [[CrossRef](#)] [[PubMed](#)]
34. Stewart, M.; Capon, R.J.; Lacey, E.; Tennant, S.; Gill, J.H. Calbistrin E and two other new metabolites from an Australian isolate of *Penicillium striatisporum*. *J. Nat. Prod.* **2005**, *68*, 581–584. [[CrossRef](#)]
35. Chen, X.-H.; Zhou, G.-L.; Sun, C.-X.; Zhang, X.-M.; Zhang, G.-J.; Zhu, T.-J.; Li, J.; Che, Q.; Li, D.-H. Penicacids E–G, three new mycophenolic acid derivatives from the marine-derived fungus *Penicillium parvum* HDN17-478. *Chin. J. Nat. Med.* **2020**, *18*, 850–854. [[CrossRef](#)] [[PubMed](#)]
36. Kumla, D.; Pereira, J.A.; Dethoup, T.; Gales, L.; Freitas-Silva, J.; Costa, P.M.; Lee, M.; Silva, A.M.S.; Sekeroglu, N.; Pinto, M.M.M.; et al. Chromone derivatives and other constituents from cultures of the marine sponge-associated fungus *Penicillium erubescens* KUFA0220 and their antibacterial activity. *Mar. Drugs* **2018**, *16*, 289. [[CrossRef](#)]
37. Asiri, I.A.M.; Badr, J.M.; Youssef, D.T.A. Penicillivinacine, antimigratory diketopiperazine alkaloid from the marine-derived fungus *Penicillium vinaceum*. *Phytochem. Lett.* **2015**, *13*, 53–58. [[CrossRef](#)]
38. Xian, P.J.; Chen, H.Y.; Feng, Z.; Zhao, W.; Yang, X.L. Capsulactone: A new 4-hydroxy- $\alpha$ -pyrone derivative from an endophytic fungus *Penicillium capsulatum* and its antimicrobial activity. *J. Asian Nat. Prod. Res.* **2021**, *23*, 1100–1106. [[CrossRef](#)] [[PubMed](#)]
39. Betina, V.; Nemeč, P.; Dobias, J.; Baráth, Z. Cyanein, a New Antibiotic from *Penicillium cyaneum*. *Folia Microbiol.* **1962**, *7*, 353–357. [[CrossRef](#)]
40. Sebak, M.; Molham, F.; Greco, C.; Tammam, M.A.; Sobeh, M.; El-Demerdash, A. Chemical diversity, medicinal potentialities, biosynthesis, and pharmacokinetics of anthraquinones and their congeners derived from marine fungi: A comprehensive update. *RSC Adv.* **2022**, *12*, 24887–24921. [[CrossRef](#)] [[PubMed](#)]
41. Takahashi, T.; Miyazawa, M. Synthesis and structure–activity relationships of phenylpropanoid amides of serotonin on tyrosinase inhibition. *Bioorg. Med. Chem. Lett.* **2011**, *21*, 1983–1986. [[CrossRef](#)]
42. Choi, D.Y.; Choi, H. Natural products from marine organisms with neuroprotective activity in the experimental models of Alzheimer’s disease, Parkinson’s disease and ischemic brain stroke: Their molecular targets and action mechanisms. *Arch. Pharm. Res.* **2015**, *38*, 139–170. [[CrossRef](#)]
43. Steyn, P.S. Austamide, a new toxic metabolite from *Aspergillus ustus*. *Tetrahedron Lett.* **1971**, *12*, 3331–3334. [[CrossRef](#)]
44. Su, Y.T.; Chang, H.L.; Shyue, S.K.; Hsu, S.L. Emodin induces apoptosis in human lung adenocarcinoma cells through a reactive oxygen species-dependent mitochondrial signaling pathway. *Biochem. Pharmacol.* **2005**, *70*, 229–241. [[CrossRef](#)] [[PubMed](#)]
45. Fredenhagen, A.; Mett, H.; Meyer, T.; Buchdunger, E.; Regenass, U.; Roggo, B.E.; Petersen, F. Protein Tyrosine Kinase and Protein Kinase C Inhibition by Fungal Anthraquinones Related to Emodin. *J. Antibiot.* **1995**, *48*, 1355–1358. [[CrossRef](#)]
46. Zhang, J.Y.; Tao, L.Y.; Liang, Y.J.; Yan, Y.Y.; Dai, C.L.; Xia, X.K.; She, Z.G.; Lin, Y.C.; Fu, L.W. Secalonic acid D induced leukemia cell apoptosis and cell cycle arrest of G1 with involvement of GSK-3 $\beta$ / $\beta$ -catenin/c-Myc pathway. *Cell Cycle* **2009**, *8*, 2444–2450. [[CrossRef](#)]
47. Zhang, D.; Novindri, D.; Nursid, M.; Yang, X.; Byeng, W.S. 12,13-Dihydroxyfumitremorgin C, fumitremorgin C, and brevipianamide F, antibacterial diketopiperazine alkaloids from the marine-derived fungus *Pseudallescheria* sp. *Nat. Prod. Sci.* **2007**, *13*, 251–254.
48. Zhang, F.; Chen, W.; Sun, L. LC-VWD-MS determination of three anthraquinones and one stilbene in the quality control of crude and prepared roots of *Polygonum multiflorum* Thunb. *Chromatographia* **2008**, *67*, 869–874. [[CrossRef](#)]

49. Piattelli, M.; Giudici de Nicola, M. Anthraquinone pigments from *Xanthoria parietina* (L.). *Phytochemistry* **1968**, *7*, 1183–1187. [[CrossRef](#)]
50. Steyn, P.S. The isolation, structure and absolute configuration of secalonic acid D, the toxic metabolite of *Penicillium oxalicum*. *Tetrahedron* **1970**, *26*, 51–57. [[CrossRef](#)]
51. Santini, A.; Mikušová, P.; Sulyok, M.; Krska, R.; Labuda, R.; Šrobárová, A. *Penicillium* strains isolated from Slovak grape berries taxonomy assessment by secondary metabolite profile. *Mycotoxin Res.* **2014**, *30*, 213–220. [[CrossRef](#)]
52. Kovács, Z.; Dinya, Z.; Antus, S. LC-SSI-MS Techniques as Efficient Tools for Characterization of Nonvolatile Phenolic Compounds of a Special Hungarian Wine. *J. Chromatogr. Sci.* **2004**, *42*, 125–129. [[CrossRef](#)] [[PubMed](#)]
53. Wang, Q.X.; Bao, L.; Yang, X.L.; Guo, H.; Yang, R.N.; Ren, B.; Zhang, L.X.; Dai, H.Q.; Guo, L.D.; Liu, H.W. Polyketides with antimicrobial activity from the solid culture of an endolichenic fungus *Ulocladium* sp. *Fitoterapia* **2012**, *83*, 209–214. [[CrossRef](#)] [[PubMed](#)]

**Disclaimer/Publisher’s Note:** The statements, opinions and data contained in all publications are solely those of the individual author(s) and contributor(s) and not of MDPI and/or the editor(s). MDPI and/or the editor(s) disclaim responsibility for any injury to people or property resulting from any ideas, methods, instructions or products referred to in the content.